On the Buoyancy Forcing and Residual Circulation in the Southern Ocean: The Feedback from Ekman and Eddy Transfer

GUALTIERO BADIN AND RICHARD G. WILLIAMS

Department of Earth and Ocean Sciences, University of Liverpool, Liverpool, United Kingdom

(Manuscript received 24 June 2008, in final form 8 June 2009)

ABSTRACT

The effect of buoyancy forcing on the residual circulation in the Southern Ocean is examined in two different ways. First, the rates of water-mass transformation and formation are estimated using air–sea fluxes of heat and freshwater in the isopycnal framework developed by Walin, which is applied to two different air–sea flux climatologies and a reanalysis dataset. In the limit of no diabatic mixing and at a steady state, these air–sea flux estimates of water-mass transformation and formation are equivalent to estimating the residual circulation and the subduction rates in the upper ocean, respectively. All three datasets reveal a transformation of dense to light waters between $\sigma = 26.8$ and 27.2, as well as positive formation rates peaking at $\sigma = 26.6$, versus negative rates peaking at $\sigma = 27$. The transformation is achieved either by surface heating or freshwater inputs, although the magnitude of the formation rates varies in each case. Second, an idealized model of a mixed layer and adiabatic thermocline for a channel is used to illustrate how changes in ocean dynamics in the mixed layer and freshwater fluxes can modify the buoyancy fluxes and, thus, alter the residual circulation. Increasing the Ekman advection of cold water northward enhances the air–sea temperature difference and the surface heat flux into the ocean, which then increases the residual circulation; an increase in wind stress of 0.05 N m^{-2} typically increases the surface heat flux by 8 W m^{-2} and alters the peaks in formation rate by up to 8 Sv (1 Sv $\equiv 10^6$ m^3 s^{-1}). Conversely, increasing the eddy advection and diffusion leads to an opposing weaker effect; an increase in the eddy transfer coefficient of 500 m^2 s^{-1} decreases the surface heat flux by 3 W m^{-2} and alters the peaks in formation rate by 1 Sv.

1. Introduction

The overturning circulation is a consequence of contrasts in surface buoyancy forcing, involving an air–sea exchange between surface waters and the overlying atmosphere. Walin (1982) provided a clear theoretical framework setting out how air–sea heat fluxes and interior mixing lead to an area-integrated transformation of warm to cold water across a temperature layer. Despite the local uncertainty in air–sea fluxes, Speer and Tziperman (1992) extended this framework to diagnose plausible rates of mode water formation in the North Atlantic from area-averaged density fluxes.

In the Southern Ocean, the overturning circulation is part of a residual circulation involving a northward transport of Subantarctic Mode Water and Antarctic Intermediate Water and a southward transport of Upper-Circumpolar Deep Water. In a similar manner to the overturning in a basin, this residual circulation across a channel requires a buoyancy forcing for a steady state to be achieved, as emphasized by a wide range of idealized and inverse model studies, including the role of eddies (Marshall 1997; Speer et al. 2000; Karsten and Marshall 2002; Marshall and Radko 2003; Olbers and Visbeck 2005; Marshall and Radko 2006). In particular, there needs to be a surface heating or freshwater input for the Upper-Circumpolar Deep Water to become transformed to lighter waters.

In this study, the residual circulation in the Southern Ocean is examined in two different ways. First, the Walin (1982) framework is applied to diagnose the transformation and formation rates in the Southern Ocean from air–sea heat and freshwater fluxes, extending the inverse studies of Speer et al. (2000) and Sloyan and Rintoul (2001). The surface density flux is diagnosed from two climatologies—National Oceanography Centre, Southampton (NOCS; Josey et al. 1998; Grist and

Corresponding author address: Gualtiero Badin, Dept. of Earth and Ocean Sciences, University of Liverpool, Liverpool, L69 3GP, United Kingdom.
E-mail: gualti@liverpool.ac.uk

DOI: 10.1175/2009JPO4080.1

Josey 2003), and Comprehensive Ocean–Atmosphere Data Set (COADS; da Silva et al. 1995a,b)—as well as from the National Centers for Environmental Prediction–National Center for Atmospheric Research (NCEP–NCAR) weather center reanalysis (Kalnay et al. 1998). Second, a conceptual model is developed to understand the effect of the heat fluxes, which can be altered by the surface feedback from ocean dynamics and the freshwater fluxes on the overturning circulation, applying residual-mean circulation theory (Andrews and McIntyre 1976; Andrews et al. 1987; Marshall and Radko 2003, 2006). In our study, the approach of Marshall and Radko (2003) is extended by including freshwater fluxes and the results are interpreted using the Walin (1982) framework. In this conceptual model, the surface heating alters according to the air–sea temperature difference, which is modified by the strength of the northward Ekman transport versus the eddy advection and diffusion. The surface density forcing is then affected by this thermal forcing and different choices for the freshwater forcing at the surface, which in turn feedback on the residual circulation.

The paper is structured as follows: The Walin (1982) framework is applied to the Southern Ocean to highlight the role of the air–sea heat and freshwater fluxes in driving water-mass formation (section 2). In the limit of no interior diabatic mixing and a steady state, this estimate of water-mass transformation is equivalent to estimating the residual circulation directed across isopycnals in the upper ocean. To complement this diagnostic view based on the data, a conceptual model is developed to solve for the residual circulation across a zonal front in an idealized representation of the Southern Ocean, where the surface fluxes vary with the Ekman transfer and eddy advection and diffusion, while different choices for the freshwater fluxes are imposed at the sea surface (section 3). Finally, the implications of the study are discussed for the Southern Ocean, and analogies are presented for how buoyancy forcing and the residual circulation operate in the shelf seas (section 4).

2. Water-mass transformation in the Southern Ocean

The rate at which water masses are transformed from one density class to another by air–sea heat and freshwater fluxes in the upper ocean is now addressed. The theoretical framework is first presented and then climatological estimates for the water-mass transformation are provided for the Southern Ocean.

a. Theoretical background

Following Walin (1982) and Nurser et al. (1999), consider a volume of fluid ΔV bound by the ρ and $\rho + \Delta\rho$ isopycnals, with an upper boundary given by the sea surface and an open boundary where the volume is connected to the rest of the ocean interior (Fig. 1).

The rate of formation of water mass $M(\rho)$ in the density interval $\Delta\rho$ is defined as the convergence of diapycnal volume fluxes $G(\rho)$ (Fig. 1a), given by

$$M(\rho)\Delta\rho = -\Delta\rho\frac{\partial G}{\partial\rho}, \tag{1}$$

which equates to the volume flux exiting the domain between the ρ and $\rho + \Delta\rho$ surfaces, plus the surface volume flux supplied by the freshwater input at the density outcrops. The diapycnal volume flux or transformation G is defined as

$$G(\rho) = \frac{1}{\Delta\rho}\int_{\text{outcrop}} D_{\text{in}}\, dA - \frac{\partial D_{\text{diff}}}{\partial\rho}, \tag{2}$$

where D_{diff} is the diffusive density flux, and D_{in} is the surface density flux into the ocean (Fig. 1b) given by

$$D_{\text{in}} = -\frac{\alpha}{C_p}H + \beta\rho_0 S(E - P), \tag{3}$$

where the surface heat flux $H(x, y)$ is positive when directed into the ocean; $E(x, y)$ and $P(x, y)$ are the evaporation and precipitation rates, respectively; $C_p(T)$ is the heat capacity for seawater at constant pressure; $\alpha(T)$ and $\beta(T)$ are the temperature dependent thermal expansion and the haline contraction coefficients of seawater, respectively; $S(x, y)$ is the salinity; and $\rho_0 = 1027$ kg m^{-3} is a reference density.

A diapycnal volume flux directed from light to dense water $G(\rho) > 0$ requires a density supply either from the surface input of density $\int_{\text{outcrop}} D_{\text{in}}\, dA > 0$ or from a convergence of diffusive density fluxes $-\partial D_{\text{diff}}/\partial\rho > 0$. Following (1), this diapycnal volume flux then creates a formation of water in a denser class (where there is convergence) and a loss (or consumption) of water in a lighter class (where there is divergence).

In the following diagnostic calculations for the Southern Ocean, the contribution to the transformation and formation from air–sea fluxes $\int_{\text{outcrop}} D_{\text{in}}\, dA$ is estimated, which may be augmented by a diffusive contribution to provide the actual transformation in the upper ocean $G(\rho)$.

In the limit of diffusive fluxes being neglected, these estimates of transformation and formation rates are equivalent to estimating the residual circulation crossing a density surface within the mixed layer and the area-integrated subduction rate from the mixed layer between the ρ and $\rho + \Delta\rho$ surfaces, respectively.

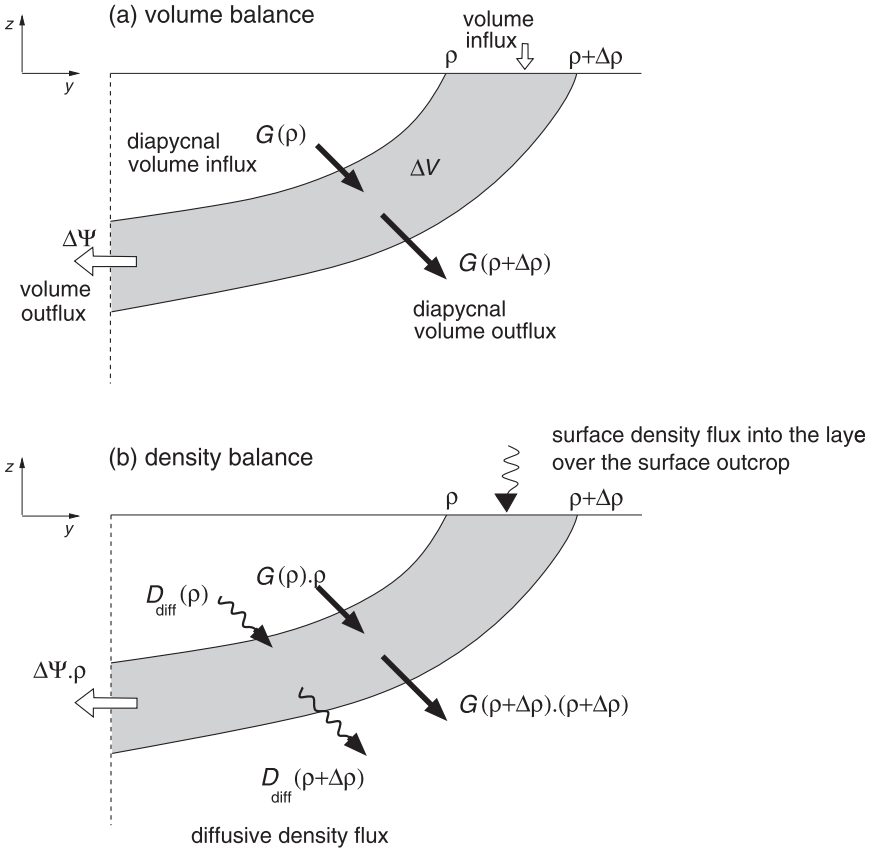

FIG. 1. Schematic vertical sections showing (a) the volume and (b) the density balances for a volume element bounded by the density surfaces ρ and $\rho + \Delta\rho$, which outcrop at the sea surface. The volume balance depends on the diapycnal volume fluxes G the volume outflux $\Delta\psi$, and the volume influx over the surface outcrop from freshwater fluxes. The density content of the layer depends on the advective change from the diapycnal volume flux ρG, the mass exiting the domain $\rho\Delta\psi$, the density gained from the atmosphere from the surface density flux over the surface outcrop $\int_{\text{outcrop}} D_{\text{in}}\, dA$, and the difference in the diffusive density fluxes across the layer D_{diff}. Modified from Nurser et al. (1999).

b. Southern Ocean data analysis

The surface density fluxes over the Southern Ocean are compared from three sources: the NOCS climatology (Josey et al. 1998; Grist and Josey 2003), the COADS climatology (da Silva et al. 1995a,b) previously analyzed by Speer et al. (2000), and the NCEP–NCAR weather center reanalysis (Kalnay et al. 1998). The NOCS climatology covers the 1980–93 period at $1° \times 1°$ resolution, while the COADS climatology extends from 1945 to 1993 at the same resolution but requires a correction to the freshwater fluxes of 1 mm day^{-1} over the denser σ classes following Speer et al. (2000). The NCEP–NCAR reanalysis is chosen to cover the same period of the NOCS climatology but employs a lower $2° \times 2°$ resolution. The surface density field is obtained from the *World Ocean Atlas* (Boyer et al. 2002; Stephens et al. 2002), with $1° \times 1°$ resolution. As the surface density flux is often dominated by the heat contribution, the maps of the surface density flux are plotted in terms of an equivalent heat flux, where a positive value represents a lightening from surface heat gain or freshwater input (Fig. 2), given by

$$H^* = H - \frac{\beta\rho_0 SC_p}{\alpha}(E - P), \tag{4}$$

so that $D_{\text{in}} \equiv -(\alpha/C_p)H^*$, where α, β, and C_p are evaluated using monthly T and S. Equivalently, D_{in} can be reinterpreted as a buoyancy flux, as $B_{\text{in}} \equiv -(g/\rho_0)D_{\text{in}} \equiv (g\alpha/\rho_0 C_p)H^*$.

In all of the climatologies there are regions of strong surface heat loss, $H^* \approx -100$ W m^{-2}, where the air passes from the land over warm ocean currents (Figs. 2a–c, dark shading), such as the Agulhas Current off South Africa, along the Brazil Current off South America, and

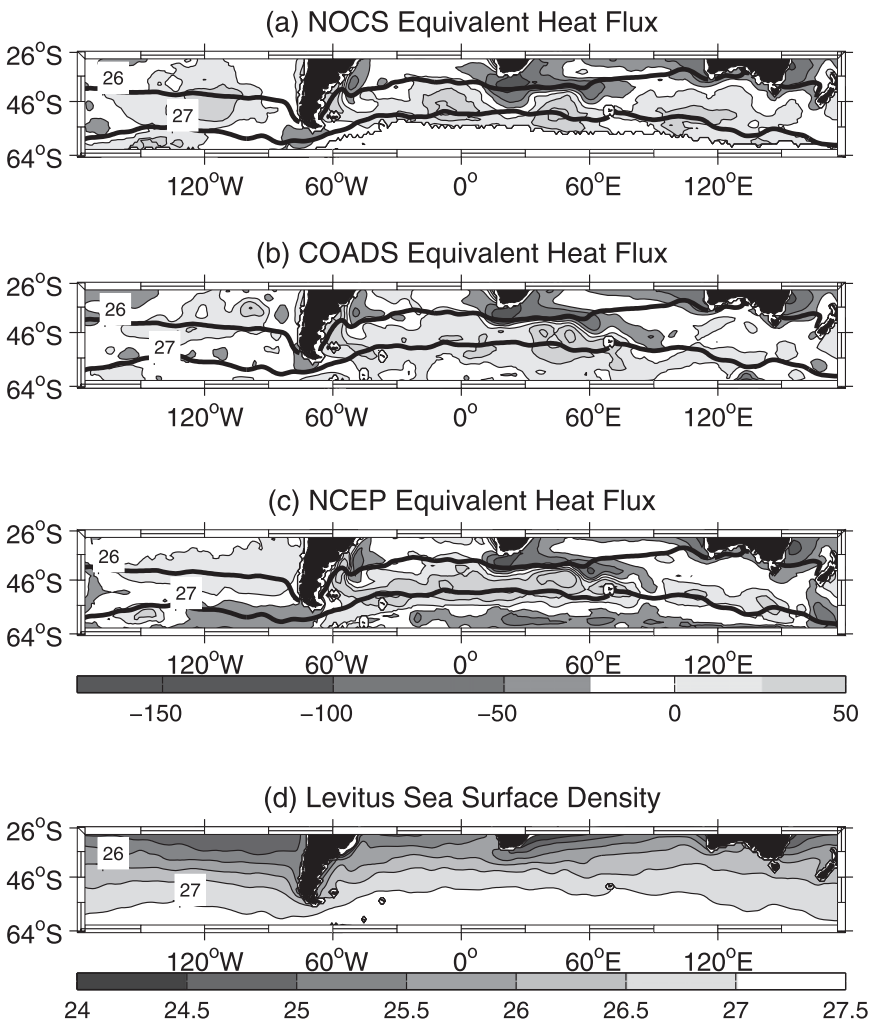

FIG. 2. Surface density flux out of the Southern Ocean expressed as an equivalent heat flux (W m^{-2}) into the ocean from the (a) NOCS, (b) COADS climatologies, (c) NCEP reanalysis, and (d) the density from the World Ocean data. Solid lines represent the $\sigma = 26$ and $\sigma = 27$ outcrops for an annual mean.

off Australia. These regions are characterized by recirculating gyres and meridional boundary currents.

In contrast, there are regions of weaker surface density lightening, $H^* < 25\,\mathrm{W\,m^{-2}}$ (Figs. 2a–c, light shading), associated with either warming or freshwater input, in the Atlantic–Indian and eastern Pacific sectors of the Southern Ocean. These regions are characterized by the flow passing through Drake Passage and the air being in a marine environment without recent contact with the land.

Now consider the area-averaged surface density fluxes over the Southern Ocean.

1) AREA-AVERAGED SURFACE FLUXES

Surface density fluxes are collected into monthly means based upon area averaging between density outcrops for each month, then combined into annual means (rather than using Eulerian means). The diagnostics are evaluated over the potential density range $25 \le \sigma \le 27.2$ using a density interval of $\Delta\sigma = 0.2$, where the potential density has been evaluated using the surface as a reference level. The range $26.5 \le \sigma \le 27.2$ is of particular interest beacuse it includes the surface outcrops of the Antarctic Circumpolar Current (ACC), but it avoids the basin regime where there are gyres and meridional boundary currents (Fig. 2d).

In the NOCS climatology, the annual surface-averaged density flux H^*_{tot} varies from density gain for lighter σ classes to lightening for denser σ classes (Fig. 3a): H^*_{tot} varies from -35 W m^{-2} at $\sigma = 25$, changing signs at $\sigma = 26.5$, and reaching 8 W m^{-2} at $\sigma = 27.2$.

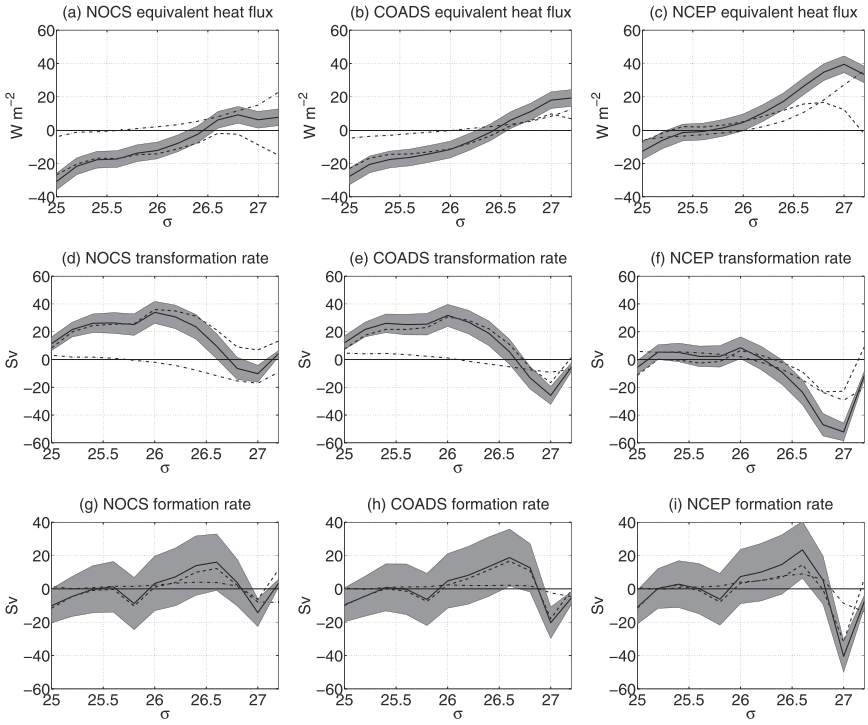

FIG. 3. Walin diagnostics from (left) NOCS, (middle) COADS, and (right) NCEP climatologies for (top) the equivalent heat flux into the ocean (W m^{-2}), (middle) diapycnal volume flux or transformation rate (Sv), and (bottom) formation rates (Sv) within a density bin of $\Delta\sigma = 0.2$. The gray area represents the change in the total density fluxes, transformation, and formation rates resulting from a ± 5 W m^{-2} variation in the heat component of the density fluxes.

The air–sea heat flux and freshwater flux provide opposing contributions to density. The surface heat flux H^*_{heat} provides a cooling everywhere (Fig. 3a, dashed line), showing an increasing trend from -25 W m^{-2} at $\sigma = 25$ to -2 W m^{-2} at $\sigma \approx 26.7$ and then decreases again to -18 W m^{-2} at $\sigma = 27.2$. In contrast, the contribution of the surface freshwater flux provides a lightening (Fig. 3a, dash–dot line) equivalent to $H^*_{\text{fresh}} \approx 22\,\text{W}\,\text{m}^{-2}$ at $\sigma = 27.2$. The trend of H^*_{tot} is controlled primarily by the surface cooling for the range $\sigma = 25$–26, but then by the freshwater input.

In comparison, in the COADS climatology, H^*_{heat} has a greater range with a density loss equivalent to 20 W m^{-2} at $\sigma = 27.2$ (Fig. 3b), which is due to comparable contributions of surface heat and freshwater input for $\sigma > 26.5$.

The NCEP reanalysis differs from both the NOCS and COADS climatologies, with a greater surface heat, particularly for $\sigma > 26$, and for larger values of freshwater input for denser σ classes (Fig. 3c).

These air–sea flux estimates reveal different regimes over the Southern Ocean. For the light surfaces $\sigma = 25$–26.5, for the NOCS and COADS datasets there is surface heat loss and density gain, associated with the presence of warm boundary currents and gyre circulations. For denser surfaces $\sigma = 26.5$–27.2, there are regions of lightening achieved either by freshwater input as in the NOCS climatology or by a combination of surface heating and freshwater input, as in the COADS and NCEP analyses. This diagnosed ocean heat gain from the atmosphere at high latitudes is rather surprising but might result from how air and sea temperatures deviate from zonal symmetry (Toole 1981; Speer et al. 2000); this aspect is investigated further in the idealized model in section 3.

2) TRANSFORMATION ESTIMATES

The contribution of air–sea fluxes to the diapycnal volume fluxes or transformation rates (2) is now diagnosed for each of the datasets. The annual transformation rate is evaluated by summing each of the monthly transformations from the surface density forcing over the monthly outcrop (Figs. 3d–f), rather than by applying an Eulerian annual average of the surface density flux over an annual outcrop.

The total annual transformation rate, G, for the NOCS climatology reveals two peaks, a positive peak with 35 Sv (1 Sv $\equiv 10^6$ m^3 s^{-1}) transformed to denser waters at

$\sigma = 26$ and a negative peak with 10 Sv transformed to lighter waters at $\sigma = 27$ (Fig. 3d, continuous line). These different directions of the transformation correspond to different regimes. Along the $\sigma = 26$ outcrop, there is intense cooling of the ocean associated with western boundary and gyre dynamics, localized, for example, over the Agulhas Current off South Africa, over the Brazil Current off South America, and off the Australian continent (Fig. 2a). In contrast, along the $\sigma = 27$ outcrop, there is a channel regime with fluid passing through Drake Passage and surface waters lightening from freshwater input over the Atlantic–Indian and east Pacific sectors of the Southern Ocean. To convey some idea of the uncertainty in the transformation diagnostics, a consistent ± 5 W m^{-2} is added to the background surface heating fields (Fig. 3, gray shades), although the actual uncertainty is probably conveyed more by the range in our diagnosed estimates from each data source.

The transformation from air–sea density fluxes G can be separated into the thermal and freshwater components, G_{heat} and G_{fresh}, respectively, which reveals that the surface heating provides the dominant contribution between $25 \leq \sigma \leq 26$, while freshwater input becomes increasingly important for denser surfaces. In particular, the freshwater component is crucial for the transformation of water masses to lighter potential density classes at $\sigma = 27$ (Fig. 3d).

Both the transformation rates diagnosed from COADS and NCEP are broadly similar to that from the NOCS climatology: transformation to denser classes at $\sigma = 26$ and to lighter classes at $\sigma = 27$ (Figs. 3e,f). The COADS transformation rates reveal a positive peak of 32 Sv at $\sigma = 26$ and a negative peak of -25 Sv at $\sigma = 27$. The main difference with the NOCS climatology lies in the lower value of G_{fresh} compared to G_{heat} at $\sigma = 27$. The NCEP transformation rates show instead a greater range in magnitudes with a peak of 10 Sv at $\sigma = 26$ and a perhaps less plausible stronger transformation to lighter waters of -50 Sv at $\sigma = 27$.

3) WATER-MASS FORMATION ESTIMATES

The contribution of air–sea density fluxes to water-mass formation is estimated from the convergence of the transformation rates over a density bin of size $\Delta\sigma = 0.2$ (1), which again neglect any contribution from interior diapycnal mixing. The formation rates have a broadly similar pattern in density space for each dataset, but there are differences in the magnitudes (Figs. 3g–i). For the NOCS climatology, the formation rates show a positive peak of 16 Sv at $\sigma = 26.6$ and two negative peaks of -10 Sv at $\sigma = 25.8$ and -15 Sv at $\sigma = 27$.

Separating the formation rate into its surface heating and freshwater contributions reveals that the thermal contribution generally dominates, which reflects how there are more abrupt changes in the thermal forcing in density space compared with the smoother changes in freshwater forcing. This diagnostic should not, though, be misinterpreted as indicating that freshwater fluxes are not important, as they dominate the transformation along denser σ surfaces.

In a comparison of the COADS climatology and NCEP reanalysis, there are stronger negative peaks in formation at $\sigma = 27$, reaching ≈ -40 Sv for the NCEP reanalysis and weaker values for the negative peak at $\sigma \approx 25.8$.

In the analysis of the formation rates, the freshwater influx at the sea surface (Fig. 1a) has been neglected in the volume balance because it only provides a minor contribution, even for the case with stronger freshwater forcing. Here, represented by the NCEP–NCAR dataset, the freshwater influx at the sea surface gives a maximum formation rate of only 0.02 Sv and a maximum consumption of only -0.2 Sv.

4) IMPLICATIONS OF THE WALIN DIAGNOSTICS

The large-scale patterns of buoyancy forcing combined with density outcrops imply transformation of dense to lighter waters in the potential density interval $26.8 \leq \sigma \leq 27.2$, peaking at $\sigma = 27$. The corresponding formation rates indicate a formation of light water of 16 Sv at $\sigma = 26.6$ and a consumption of dense water of -15 Sv at $\sigma = 27$.

However, the three datasets show a different role for the separate heat and freshwater components of the fluxes. In the NOCS climatology, there is a surface cooling and the lightening is provided by freshwater input. In contrast, in the COADS and NCEP datasets, the lightening of dense water is achieved by a combination of surface warming and freshwater input.

Our transformation estimates also neglect the effect of diapycnal mixing and include systematic errors from the air–sea flux climatologies over the Southern Ocean. While accepting the limitations of our diagnostics calculations, they have highlighted the role of the air–sea density fluxes in driving a water-mass conversion over the Southern Ocean. The water-mass transformation and formation estimates are diagnostics, so they are unable to tell us about the role that the dynamics play in determining the water masses. This issue is now addressed using an idealized model of the mixed layer and upper thermocline in the Southern Ocean.

3. What sets the buoyancy fluxes?

The previous diagnostics of the air–sea density fluxes over the Southern Ocean, particularly the high-latitude

lightening, pose the following questions: How are these fluxes controlled? Are the surface fluxes simply driven by thermodynamical exchanges dictated by the large-scale atmospheric patterns or is there a feedback from ocean dynamics? In turn, how does the variation in these air–sea fluxes affect the residual circulation?

To investigate how the residual circulation depends on the closure for the surface density fluxes, a zonally averaged channel model is considered, consisting of a surface diabatic mixed layer overlying an adiabatic ocean interior (Fig. 4a). For an ocean channel, the solution of the problem is obtained by applying the transformed Eulerian-mean theory of Andrews and McIntyre (1976), following the method introduced by Marshall and Radko (2003).

a. Mixed layer balances

The zonally averaged mixed layer evolution for the mixed layer temperature $T_m(y,t)$ and salinity $S_m(y,t)$ are

$$\frac{\partial \overline{T_m}}{\partial t} + \frac{\partial}{\partial y}(\overline{v_m T_m} + \overline{v'_m T'_m}) = \overline{H}, \tag{5}$$

$$\frac{\partial \overline{S_m}}{\partial t} + \frac{\partial}{\partial y}(\overline{v_m S_m} + \overline{v'_m S'_m}) = \overline{F}, \tag{6}$$

where the subscript m indicates that we are considering the tracer evolution in the mixed layer, the overbars represent a mean obtained from a low-pass time-filtering operation over several baroclinic eddy life cycles, and the primes denote the deviations from the mean. Here, $\overline{H}$ and $\overline{F}$ indicate the heat and freshwater forcing, respectively. The mixed layer temperature $T_m(y, t)$ and salinity $S_m(y, t)$ are considered vertically homogeneous in the mixed layer.

The eddy fluxes $\overline{v'_m T'_m}$ and $\overline{v'_m S'_m}$ can be parameterized as

$$\overline{v'_m T'_m} = -K\frac{\partial \overline{T_m}}{\partial y} \quad \text{and} \tag{7}$$

$$\overline{v'_m S'_m} = -K\frac{\partial \overline{S_m}}{\partial y}, \tag{8}$$

where K is the eddy transfer coefficient. Following Visbeck et al. (1997), K can be parameterized as

$$K = k|s_\rho|, \tag{9}$$

where $s_\rho = \partial z_\rho/\partial y$ is the thermocline slope of the isopycnal of depth z_ρ at the base of the mixed layer, and $k = L_y K/\mathcal{H}$ is the eddy parameter.

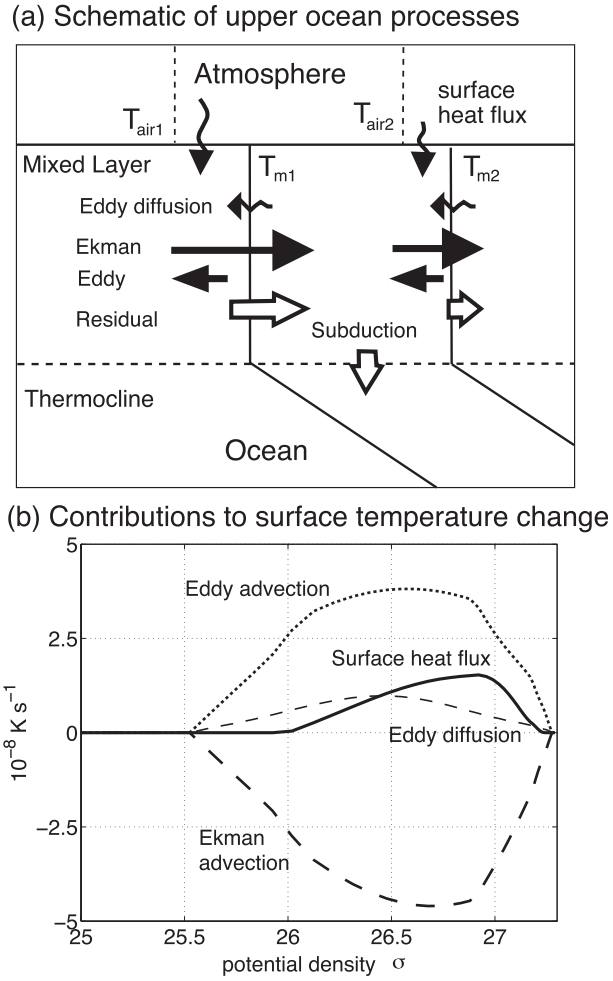

FIG. 4. The effect of ocean dynamics on surface heat flux with (a) a schematic figure denoting the processes operating in the idealized mixed layer and adiabatic thermocline model and (b) diagnostics of surface temperature rate of change from a surface heat flux dependent on the air–sea temperature difference (thick continuous line), which is affected by the Ekman transport (thick dashed line), eddy horizontal advection (dotted line), and diffusion (thin dashed line). The resulting surface buoyancy input then enables formation of water masses and subduction to occur. The partition in (b) is obtained from the idealized model in the case of no freshwater fluxes.

With the use of (9), the divergence of the eddy fluxes gives rise to the eddy advection terms $v^*(\partial T_m/\partial y)$ and $v^*(\partial S_m/\partial y)$ and the eddy diffusion terms $k|s_\rho|(\partial^2 T_m/\partial y^2)$ and $k|s_\rho|(\partial^2 S_m/\partial y^2)$. The advective role of the eddies in the mixed layer might assist in the transfer of tracers (Lee et al. 1997) and of heat (Fox-Kemper et al. 2008; Fox-Kemper and Ferrari 2008) and, thus, might affect the formation rates of water (Cerovecki and Marshall 2008). Using the transformed Eulerian-mean theory of Andrews and McIntyre (1976), we define a residual-mean advective velocity as the sum of the Ekman and eddy advection velocities,

TABLE 1. Numerical constants used in the model.

f	Coriolis parameter	-10^{-4} s^{-1}
L_x	Horizontal scale of the channel	21×10^6 m
L_y	Meridional scale of the channel	2×10^6 m
$\mathcal{H}$	Vertical scale	1000 m
h_m	Mixed layer depth	200 m
C_{pA}	Heat capacity of air	1008 J K^{-1} kg^{-1}
ρ_a	Air density	1.25 kg m^{-3}
ρ_0	Water density	1027 kg m^{-3}
c_d	Drag coefficient of the wind stress	1.3
a, b, c	Water vapor coefficients	0.7859, 0.034 77, 0.004 12
E	Relative humidity coefficient	0.621 97
τ_0	Maximum wind stress	0, 0.075, 0.1, 0.15, 0.2 N m^{-2} (default: $\tau_0 = 0.15$ N m^{-2})
K	Eddy transfer coefficient	250, 500, 1000, 1500, 2000 m^2 s^{-1} (default: $K = 500$ m^2 s^{-1})

$$v_{\mathrm{res}} = v_{\mathrm{Ek}} + v^*. \tag{10}$$

The residual circulation satisfies nondivergence,

$$\nabla \cdot v_{\mathrm{res}} = 0, \tag{11}$$

so that it is possible to define a residual-mean streamfunction,

$$\psi_{\mathrm{res}} = \psi_{\mathrm{Ek}} + \psi^*, \tag{12}$$

where $\psi_{\mathrm{Ek}} = -\tau_0/\rho_0 f$ is the meridional Ekman transport streamfunction, τ_x is the eastward wind stress, and f is the Coriolis parameter, so that $\partial\psi_{\mathrm{res}}/\partial y = w_{\mathrm{res}}$ and $-\partial\psi_{\mathrm{res}}/\partial z = v_{\mathrm{res}}$.

The residual-mean streamfunction ψ_{res} and the Eulerian-mean and eddy velocities satisfy the boundary conditions of zero normal components at solid boundaries and at the sea surface.

Given the closure for the eddy fluxes, the tracer evolution for the mixed layer [(5) and (6)] can be integrated over the mixed layer depth h_m for the mixed layer temperature and salinity, giving

$$\frac{\partial \overline{T_m}}{\partial t} + \frac{1}{h_m}(\psi_{\mathrm{res}})_{-h_m}\frac{\partial \overline{T_m}}{\partial y} = \frac{1}{\rho_0 C_p h_m}\overline{H} + k|s_\rho|\frac{\partial^2 T_m}{\partial y^2} \quad \text{and} \tag{13}$$

$$\frac{\partial \overline{S_m}}{\partial t} + \frac{1}{h_m}(\psi_{\mathrm{res}})_{-h_m}\frac{\partial \overline{S_m}}{\partial y} = \frac{S_m}{h_m}(\overline{E} - \overline{P}) + k|s_\rho|\frac{\partial^2 S_m}{\partial y^2}, \tag{14}$$

where $\overline{E}$ is the evaporation rate, and $\overline{P}$ is the precipitation rate.

The surface heat fluxes are obtained using bulk formulas based on the air–sea temperature difference (Gill 1982; Williams 1988):

$$\overline{H_{\mathrm{ir}}} = 4\sigma(\overline{T_m} - T_{\mathrm{air}})(T_{\mathrm{air}} + 273)^3, \tag{15}$$

$$\overline{H_{\mathrm{sens}}} = \rho_a A_h u_w C_{\mathrm{pA}}(\overline{T_m} - T_{\mathrm{air}}), \quad \text{and} \tag{16}$$

$$\overline{H_{\mathrm{lat}}} = 0.0015\overline{L}\rho_a u_w(\overline{r}_m - r_{\mathrm{air}}), \tag{17}$$

where $\overline{H_{\mathrm{ir}}}$, $\overline{H_{\mathrm{sens}}}$, $\overline{H_{\mathrm{lat}}}$ are the longwave radiation, sensible heat, and latent heat flux, respectively; T_{air} is the temperature of the air at the sea surface; σ is the Stefan–Boltzmann constant; ρ_a is the density of the air at the sea surface; A_h is the heat transfer coefficient, which depends on the wind speed and on the temperature difference between the sea surface and the air (Smith 1988); $u_w = \sqrt{\tau\rho_0/\rho_a c_d}$ is the wind speed, where c_d is the drag coefficient of the wind stress; C_{pA} is the heat capacity of air; $\overline{L}$ is the latent heat of evaporation, calculated as $\overline{L} = 2500800 - (2300\overline{T_m})$, so that the evaporation rate can be calculated as $\overline{E} = \overline{H_{\mathrm{lat}}}/\rho L$; r is the specific humidity, which is related to the saturated water vapor pressure $\overline{e}$, given by

$$\overline{r} = \epsilon\frac{\overline{e}}{P_a}\left[1 - \frac{\overline{e}}{P_a}(1 - \epsilon)\right]^{-1}, \tag{18}$$

where ϵ is a constant and P_a is the atmospheric pressure; and the saturated water vapor pressure e can be parameterized in function of the sea surface temperature as

$$\overline{e} = 0.98 \times 10^{(a + b\overline{T_m})/(1 + c\overline{T_m})}, \tag{19}$$

where a, b, and c are constants. The values of all the parameters employed by the model are reported in Table 1.

The model represents the heat fluxes as the fluxes being due to the mismatch of the isotherms of the ocean and the atmosphere, which results from the large-scale atmospheric forcing such as wind and the feedback from

ocean dynamics, such as Ekman and eddy fluxes (Fig. 4a). The surface density fluxes are then affected by the resulting surface heat and freshwater fluxes. The mixed layer temperature, thus, receives a negative contribution from the Ekman flux because of the transfer of cold water from the polar regions, opposed by the action of the eddy advection and diffusion, which results in a heat exchange with the atmosphere (Fig. 4b). In comparison, Marshall and Radko (2006) also used interactive heat fluxes with a simpler Newtonian relaxation to a background buoyancy.

The model is allowed to evolve until (13) and (14) reach a steady state. Surface fluxes are then obtained in an iterative manner:

1) The mixed layer temperature is initialized with the imposed air temperature, which is kept constant in time, such that $T_m(y, 0) = T_{\text{air}}(y)$. The mixed layer temperature is always relaxed to the air temperature at the meridional boundaries, so that $T_m(0, t) = T_{\text{air}}(0)$ and $T_m(L_y, t) = T_{\text{air}}(L_y)$. The mixed layer salinity is fixed at the meridional boundaries as well, so that $S_m(0, t) = S_m(0, 0)$ and $S_m(L_y, t) = S_m(L_y, 0)$. The air temperature increases from 1° to 12°C northward across the channel. and the mixed layer salinity is initialized to increase from 34 to 35.
2) A wind stress of the form

$$\tau(y) = \tau_0 \sin\left(\frac{\pi y}{L_y}\right) \tag{20}$$

is imposed, as well as a constant mixed layer thickness h_m and a first guess for the isotherm slope at the base of the mixed layer. The wind stress forcing is centered at the middle of the channel and reduces to zero 1000 km on either side.
3) The surface heat flux and the evaporation rate are obtained from the mismatch of the ocean to the atmosphere isotherms. Different choices of $E - P$ are imposed.
4) The density at the base of the mixed layer is calculated from $\overline{T_m}$ and $\overline{S_m}$ using the linear approximation for the equation of state for seawater:

$$\Delta\overline{\rho_m} = -\alpha\rho_0\Delta\overline{T_m} + \beta\rho_0\Delta\overline{S_m}. \tag{21}$$

The knowledge of the surface fluxes and mixed layer density provide the upper-boundary conditions for the thermocline.

To close for the slope of the isopycnals at the base of the mixed layer, which defines the advection and diffusion in (13) and (14), the interior dynamics needs to be considered.

b. Thermocline balances

The thermocline is assumed to be adiabatic, with eddies acting to advect tracers along isopycnals.

The knowledge of density at the base of the mixed layer and of the total density fluxes D_{in} allows the residual streamfunction to be calculated at the base of the mixed layer as

$$(\psi_{\text{res}})_{-h_m} = \frac{D_{\text{in}}}{(\partial\overline{\rho_m}/\partial y)}. \tag{22}$$

Following Visbeck et al. (1997), the interior eddy streamfunction is parameterized as

$$\psi^* = k\left|\frac{\partial z_\rho}{\partial y}\right|\frac{\partial z_\rho}{\partial y} = k|s_\rho|s_\rho. \tag{23}$$

Combining (12), (22), and (23) and rearranging gives a relationship between thermocline slope, wind stress, and the strength of the residual circulation as

$$\frac{\partial z_\rho}{\partial y} = -\left[-\frac{\tau}{k\rho_0 f} - \frac{1}{k}\psi_{\text{res}}(\overline{\rho_m})\right]^{1/2}, \tag{24}$$

where the negative sign is chosen to reproduce the observed slope of the isopycnals in the Southern Ocean.

c. Idealized model solutions for different choices of freshwater forcing

The effect of the interactive surface forcing is assessed in the idealized model for three different choices of freshwater fluxes: no freshwater forcing, and $\overline{E} - \overline{P}$ prescribed from the NOCS and NCEP datasets, respectively, assuming a maximum wind stress τ_0 of 0.15 N m^{-2}.

The surface heat fluxes arise from the mismatch of the ocean and atmosphere isotherms. The partition of the change of the mixed layer temperature, for the case without freshwater forcing (Fig. 4b), shows that the air–sea heat flux arises from the northward advection of cold water by the Ekman term, which is only partially opposed by a southward transfer of heat by the eddy advection and diffusion. Although eddy diffusion provides the smallest contribution, it is almost as large as the heat transfer by the residual circulation.

In the case of no freshwater fluxes there is a surface heat input of 12.5 W m^{-2} at the outcrop of $\sigma = 26.9$ (Fig. 5a), which increases to an effective heat flux of more than 27 W m^{-2} when including freshwater forcing (Fig. 5b).

This surface forcing leads to a transformation of dense into lighter water: for no freshwater fluxes, there is a transformation peak of -7 Sv at $\sigma = 26.8$ (Fig. 5c). When the NOCS freshwater forcing is imposed, transformation

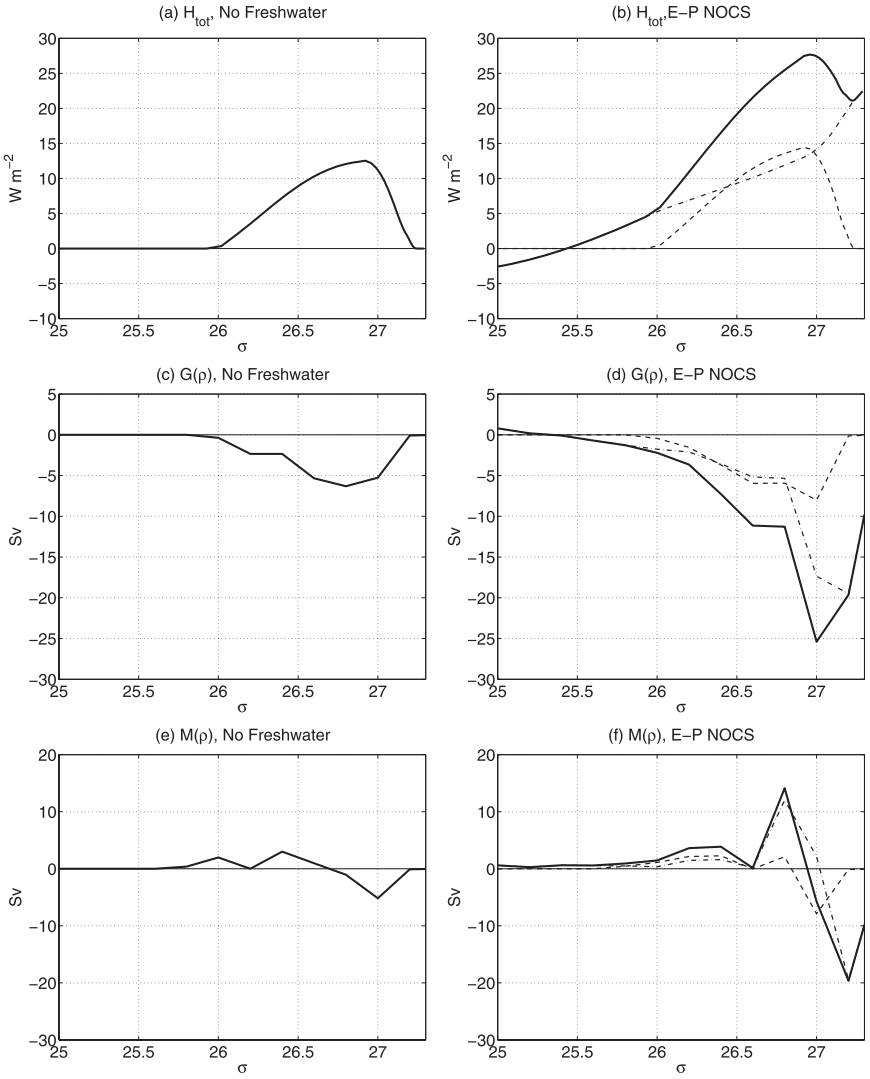

FIG. 5. Walin diagnostics for an idealized model for (top) the equivalent heat fluxes (W m^{-2}), (middle) transformation rates (Sv), and (bottom) formation rates (Sv) within a density bin of $\Delta\sigma = 0.2$. The idealized model is forced by interactive heat fluxes with (a),(c),(e) no freshwater fluxes or (b),(d),(f) NOCS freshwater fluxes. Dashed line is the heat component, dot–dashed line is the freshwater component, and the continuous line is the total flux.

rates reach higher values of −25 Sv at $\sigma = 27$ (Fig. 5d). Hence, including freshwater fluxes enhances the magnitude of the water-mass transformation and shifts their peak values to slightly denser classes by $\Delta\sigma = 0.2$.

The streamfunction for the residual circulation without freshwater forcing reveals a cell with dense water upwelling near the pole, being transformed to lighter water, and being subducted toward the equator (Figs. 6a,c)—in agreement with Karsten and Marshall (2002), Marshall and Radko (2003), and Marshall and Radko (2006). In the case with freshwater forcing from the NOCS climatology, the asymmetry in the surface density fluxes alters the residual streamfunction, making the flow more intense toward the poleward edge of the bowl containing the flow, in agreement with the poleward increase of the total fluxes due to the presence of the freshwater fluxes (Figs. 6b,d).

The surface forcing leads to water masses being formed at light density classes and consumed at dense water classes. For no freshwater fluxes, there is a formation peak of 3 Sv at $\sigma = 26.4$ and a consumption peak of −5.2 Sv at $\sigma = 27$ (Fig. 5e). When the NOCS freshwater forcing is imposed, formation rates reach higher values of 14 Sv at $\sigma = 26.8$ and the peak in consumption rate shifts to $\sigma = 27.2$ and increases in magnitude to −19.6 Sv (Fig. 5f). Hence, including freshwater fluxes

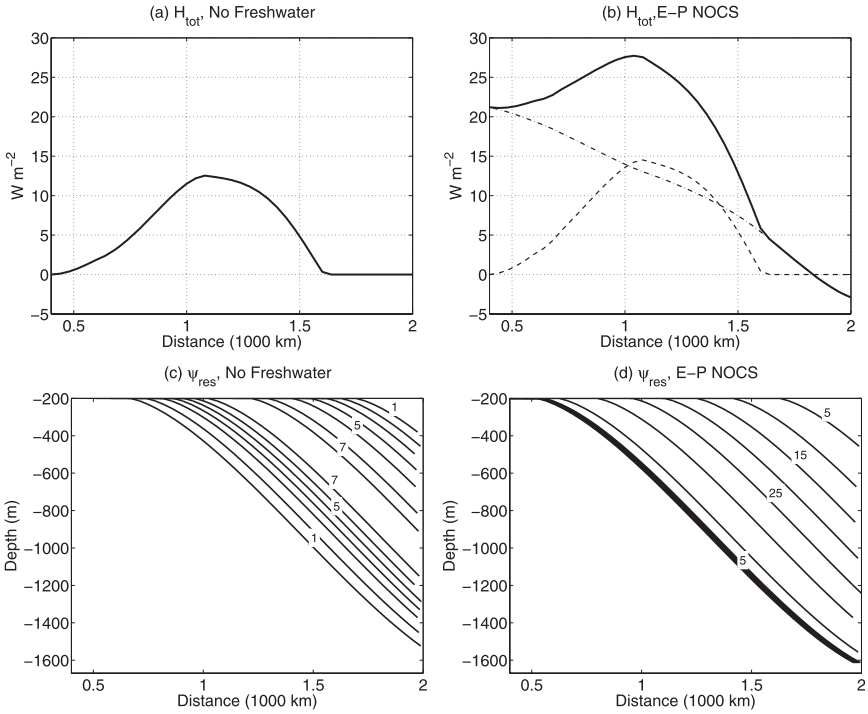

FIG. 6. (top) Surface equivalent heat flux (W m^{-2}) vs (bottom) meridional distance and section for the residual circulation (Sv) from the idealized model (a),(c) for no freshwater fluxes and (b),(d) for NOCS freshwater fluxes. Dashed line is the heat component, dot–dashed line is the freshwater component, and dark solid line in (d) is the total component of the fluxes in (b). North is to the right of the plots.

also enhances the magnitude of the water-mass formation and consumption rates and shifts their maxima and minima by $\Delta\sigma = 0.2$ to slightly denser classes.

These modeled formation rates lie within the range previously diagnosed for the Southern Ocean (Fig. 3) although the idealized models have slightly smaller equivalent heat inputs and formation rates than that for the NCEP climatology but a larger equivalent heat input than the NOCS climatology, which shifts the formation and consumption peaks to slightly denser classes. In particular, the idealized model has a surface heat input resulting from the northward displacement of the isotherms in the ocean by the residual circulation, in contrast to the surface heat loss diagnosed in the NOCS climatology.

d. The effect of ocean dynamics on the formation rates

The surface forcing is evaluated in an interactive manner within the idealized model, so that changes in ocean dynamics alter the surface temperature, which in turn alter the surface heat flux. Two separate effects are investigated here: the role of Ekman transport and eddy transfer within the surface mixed layer.

In terms of the controlling mechanisms, as the surface stress increases there is an increase in the northward Ekman advection of cold waters, which leads to a greater air–sea temperature difference and increases the surface heat flux into the ocean by typically 10 W m^{-2} (Fig. 7a). Conversely, as the rate of eddy advection and diffusion increases within the mixed layer, the northward Ekman advection of cold water is opposed by the poleward eddy advection and diffusion of heat, which reduces the air–sea temperature difference and the surface heat flux by typically -3 W m^{-2} (Fig. 7b).

These competing effects are now explored in more detail.

1) WHAT IS THE SENSITIVITY TO CHANGES IN LARGE-SCALE WIND FORCING?

Now consider the sensitivity of the surface forcing and residual circulation to changes in the magnitude of the wind stress, which is chosen to increase up to $\tau_0 = 0.2$ N m^{-2} with the same symmetric pattern within the channel.

As the strength of the wind increases, the Ekman advection increases the surface heat flux into the ocean, with its maximum value shifting slightly toward lighter

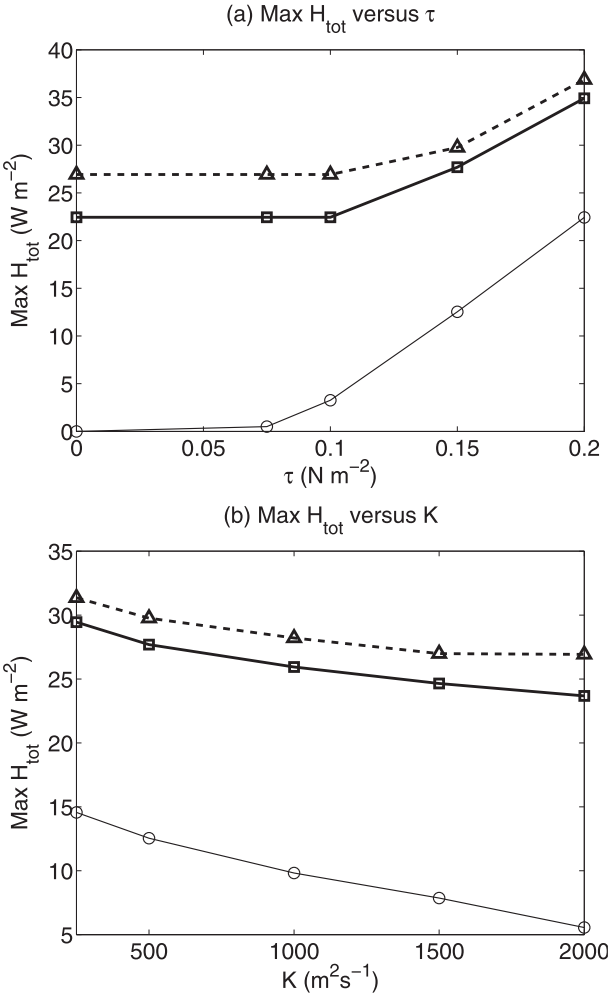

FIG. 7. The maximum in the surface equivalent heat flux (W m^{-2}) as a function of (a) wind stress τ (N m^{-2}) and (b) eddy diffusion K (m^2 s^{-1}) from the idealized model. Three cases are considered: no freshwater fluxes (thin continuous lines), freshwater forcing from NOCS (thick continuous lines), and NCEP (thick dashed lines).

density classes (Figs. 8a,b). The total equivalent heat flux increases monotonically as a function of wind stress (Fig. 7a), although the increase is reduced if there is already a freshwater input.

If there is no freshwater forcing and the maximum wind stress increases from $\tau_0 = 0.15$ to 0.2 N m^{-2}, the surface heat flux into the ocean increases by more than 10 W m^{-2}, which increases the transformation rate by -6.7 Sv and shifts the peak in the transformation to slightly denser classes of $\Delta\sigma = 0.2$ (Fig. 8c). The peaks in formation rate are increased by 2.5 Sv and consumption rate by -7.5 Sv (Figs. 8e and 9a,b). Thus, in the case with no freshwater fluxes, as the wind stress increases, the consumption rates increase faster than the formation rates.

If freshwater forcing is applied, the same increase in wind stress leads to a broadly similar increase in surface heat flux of 8 W m^{-2} but leads to a smaller increase in the peak of the transformation rate of 3 Sv and a decrease in the peak of the formation rate of 4.3 Sv.

If there is no freshwater forcing, the changes in surface heat flux (induced by variations in wind stress) are sufficiently large to alter the density class at which the peaks in formation occur; however, when the freshwater forcing is included, these changes in surface heat flux are too small to lead to the same effect and the formation rate does not monotonically increase because of the changes in the density range where the formation occurs (Figs. 8f and 9a).

2) WHAT IS THE SENSITIVITY TO CHANGES IN EDDY TRANSFER?

The sensitivity to the eddy transfer is now explored in the idealized model by altering the eddy transfer coefficient from $K = 250$ to 2000 m^2 s^{-1}.

For the case with no freshwater forcing, an increase of the eddy transfer coefficient from $K = 500$ to 1000 m^2 s^{-1} decreases the equivalent heat fluxes by 2.7 W m^{-2}, leading to only slight decreases in the magnitude of the peak in transformation rate of 1 Sv and formation rates of 1 Sv (Figs. 10a,b).

There is a similar weak response when there is freshwater forcing, with the freshwater forcing altering the monotonic decrease of the maximum of the formation rates as K decreases. Hence, interactive surface buoyancy fluxes and eddy diffusion can combine in a nonlinear manner in altering the formation rates, as speculated by Marshall and Radko (2003).

e. What is the response of the interior thermocline?

Altering the wind stress or the eddy transfer has an effect on the interior thermocline structure, based on (24). As the wind stress increases, the maximum depth of the residual circulation (24) increases monotonically when there is no freshwater forcing and the thickness of thermocline z_ρ converges to the same value (Fig. 9c).

However, this response becomes more complicated when there are freshwater fluxes resulting from their nonmonotonic effect in changing the water formation, with the maximum thermocline depth showing first a decrease and then an increase with increasing wind stress.

Changes in the eddy advection and diffusion in the mixed layer likewise affect the eddy parameter k, which controls the strength of the eddy streamfunction (23) and, thus, the depth of the residual circulation (24): increasing the eddy transfer coefficient K leads to the maximum depth of the residual circulation decreasing monotonically (Fig. 10c), although eventually the thickness of

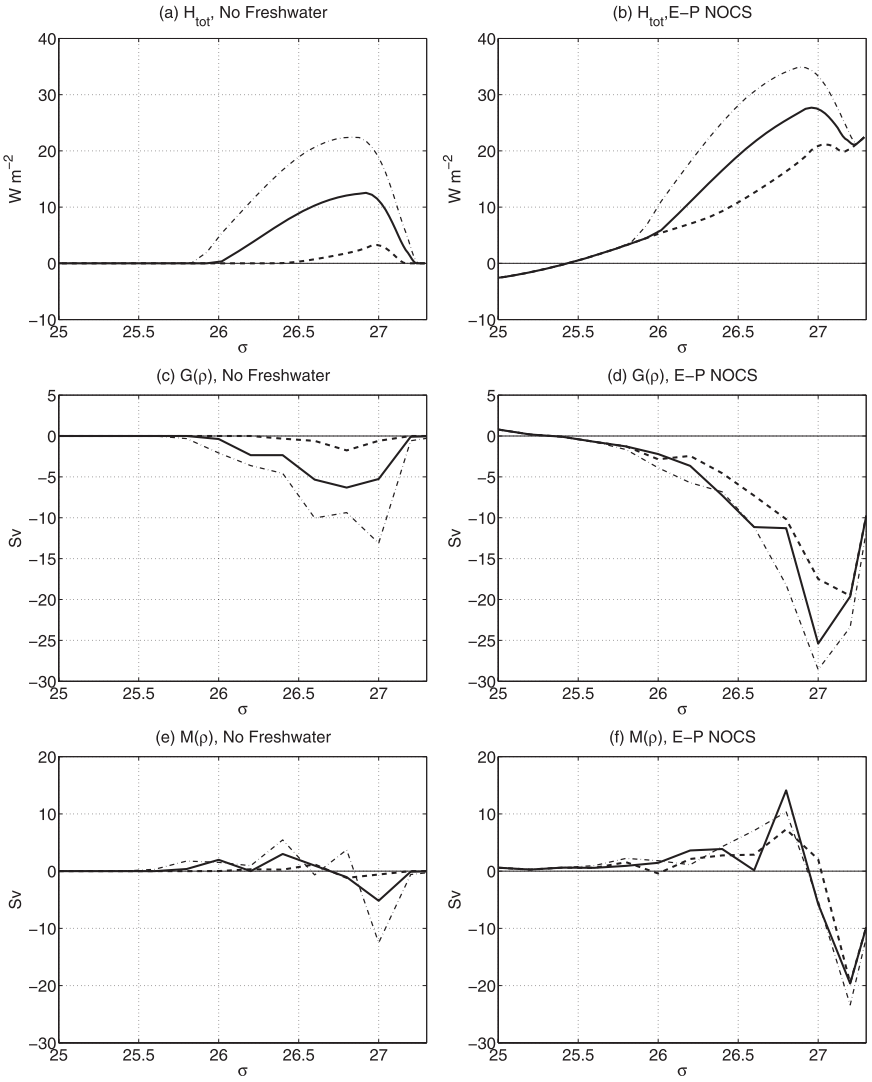

FIG. 8. Walin diagnostics for variable strength in the winds—$\tau = 0.1$ N m^{-2} (dashed line), $\tau = 0.15$ N m^{-2} (continuous line), and $\tau = 0.2$ N m^{-2} (dot–dashed line)—using the idealized model for (top) the surface equivalent heat fluxes (W m^{-2}), (middle) transformation rate (Sv), and (bottom) formation rate (Sv). Within a density bin of $\Delta\sigma = 0.2$ for the cases of (a),(c),(d) no freshwater fluxes and (b),(d),(e) NOCS freshwater fluxes.

thermocline z_ρ converges to the same value with further increases in K.

4. Discussion

The study addresses the question of how the residual circulation is controlled by surface buoyancy fluxes and altered by the thermal feedback from mixed layer dynamics.

To partly answer this question, the Walin isopycnal framework is employed, providing an elegant diagnostic link between surface density forcing and water-mass transformation for the residual circulation following Marshall (1997). Climatological diagnostics suggest that surface waters circulating the ACC are transformed from dense to light waters. The Walin approach highlights the importance of the surface density forcing, although limited knowledge of the size of the freshwater fluxes and diffuse density fluxes prevents a closer assessment of predictions from the Walin approach and independent tracer signals for the residual circulation.

Although the residual circulation has to be consistent with the surface density forcing at steady state, the surface density forcing is altered by both the large-scale forcing from the atmosphere and the feedback from sea surface temperature affected by ocean dynamics. This relationship is explored in a conceptual model for

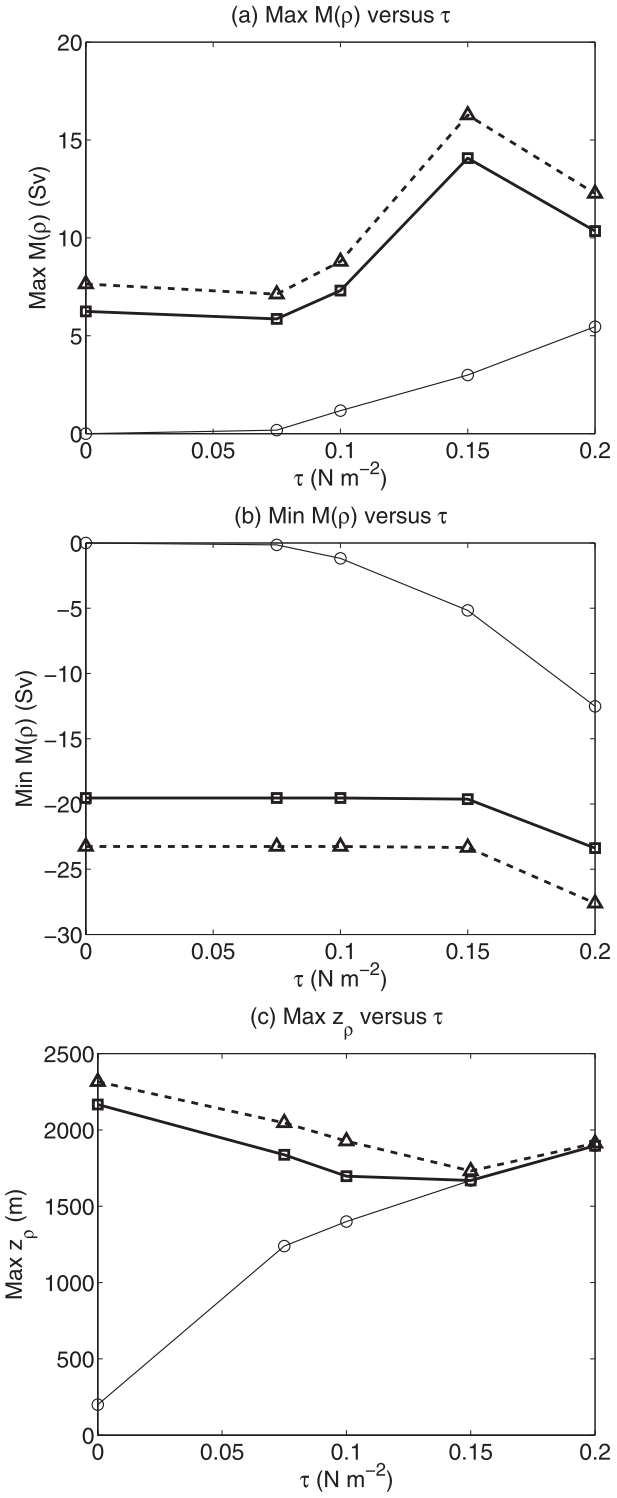

FIG. 9. The sensitivity of Walin diagnostics as a function of wind stress τ (N m^{-2}) for (a) the peak in maximum formation rate (Sv) of light water at $\sigma = 26.9$; (b) the peak in minimum formation rate (Sv), corresponding to the consumption of dense water at $\sigma = 27.2$; and (c) the maximum depth of the residual circulation (m). Three cases are considered: no freshwater fluxes (thin continuous lines), freshwater forcing from NOCS (thick continuous lines), and NCEP (thick dashed lines).

Ekman and eddy transfers within a mixed layer and adiabatic thermocline for the Southern Ocean.

Within the model framework, changes in wind stress alter the horizontal Ekman transport and the surface temperature distribution, which in turn alter the surface heat flux based upon a simple air–sea temperature difference; this viewpoint emphasizes how air–sea heat fluxes over the Southern Ocean are due to slight deviations in the alignment of air and sea temperatures following Toole (1981) and Speer et al. (2000). In the idealized model, an increase of the maximum wind stress from 0.15 to 0.2 N m^{-2} increases the surface heat fluxes by more than 10 W m^{-2}, enhancing the magnitude of peaks in formation and consumption rates by up to 8 Sv. Conversely, an increase in eddy transfer opposes the Ekman advection within the mixed layer and reduces the air–sea heat fluxes and associated formation rates; however, this feedback is relatively weak because increasing the eddy diffusivity from 500 to 1000 m^2 s^{-1} only decreases the surface heat fluxes by typically 5 W m^{-2} and reduces the formation rates by less than 3 Sv.

Even if changes in eddy advection and diffusion have a weak effect on the changes in the formation rates, eddy transfer itself plays an important role in the transfer of heat in the mixed layer, which can approach the magnitude of the heat transfer within the mixed layer by the residual circulation; this result is in agreement with that obtained in the idealized model by Marshall and Radko (2003) and in the eddy-resolving GCM by Cerovecki and Marshall (2008).

The relevance of this idealized model result for the real Southern Ocean depends on whether the lightening of the surface waters in the ACC is achieved by freshwater input or surface heating. There is no clear consensus as to which process dominates. Ocean dynamics in the mixed layer are likely to provide an important feedback to the surface forcing if the surface lightening is due to surface heating but not if the lightening is due to surface freshening linked to the atmospheric water cycle.

This example of how the residual circulation might be sensitive to both buoyancy forcing and ocean dynamics has direct analogies with other systems. In shelf seas, there are summer fronts arising from how tidal mixing is modulated by bathymetry (Simpson and Hunter 1974): tidal mixing is stronger in shallower waters leading to well-mixed, cooler onshore waters being separated from stratified, warmer surface offshore waters. As air passes over the shelf seas, the cooler onshore waters receive greater heating than the warmer offshore waters, which then drives a surface transformation of cooler to warmer waters. This transformation leads to an offshore flux across the tidally mixed front together with an opposing onshore flux of middepth waters.

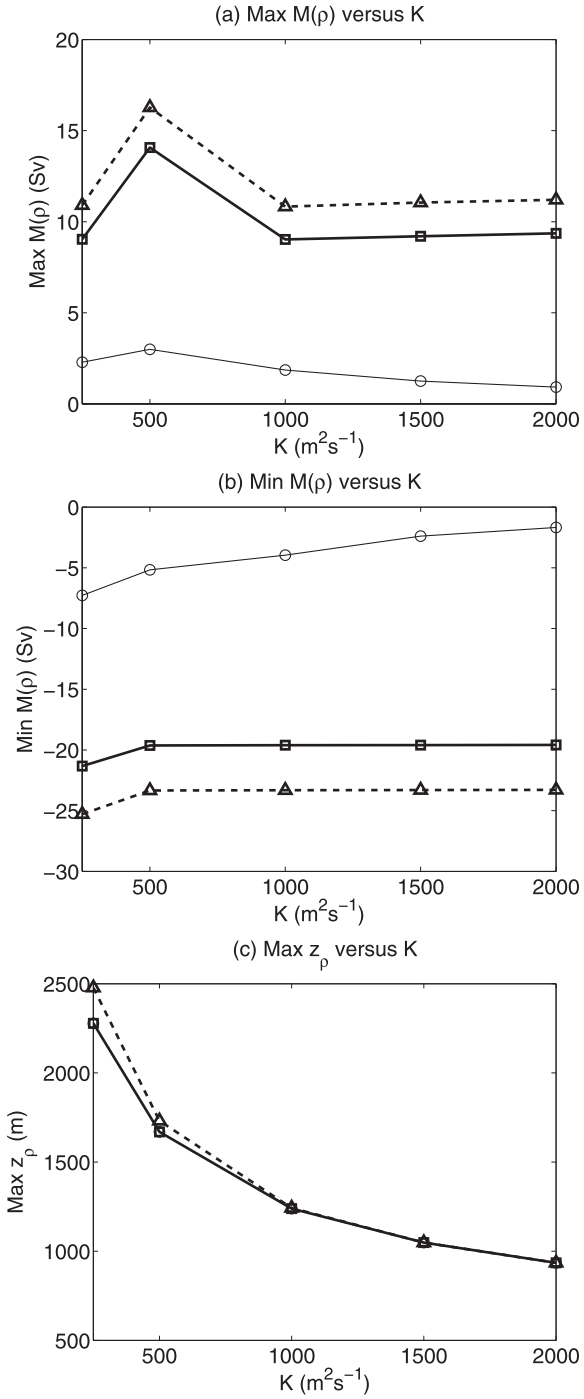

FIG. 10. Sensitivity of Walin diagnostics as a function of the eddy diffusion K (m^2 s^{-1}) for (a) the peak in maximum formation rate (Sv) of light water at σ = 26.9 m; (b) the peak in minimum formation rate (Sv), corresponding to the consumption of dense water at σ = 27.2; and (c) the maximum depth of the residual circulation (m), as a function of the eddy diffusion K (m^2 s^{-1}). Three cases are considered: no freshwater fluxes (thin continuous lines), freshwater forcing from NOCS (thick continuous lines), and NCEP (thick dashed lines). Notice that the cases with no freshwater fluxes and with freshwater forcing from NOCS are superimposed.

This debate of how the residual circulation is controlled in the Southern Ocean is important because the transfer of tracers and sequestering of gases, such as carbon dioxide, is ultimately affected by this process (Ito et al. 2004). Indeed, the recent strengthening of the winds over the Southern Ocean (Thompson and Solomon 2002) has been interpreted as weakening the ocean uptake of anthropogenic CO_2 in the Southern Ocean (LeQuere et al. 2007). Following our idealized model, an increase in the winds is indeed expected to increase the upwelling of carbon-rich waters but at the same time increase the subduction into the interior of the ocean, leading to carbon sequestration. Ultimately, the answer as to how the residual circulation adjusts to climate change and the resulting uptake of tracers depends on the precise nature of the changes in the air–sea fresh and heat fluxes, with the latter sensitive to the underlying ocean dynamics.

Acknowledgments. We are grateful to support from the U.K. Natural Environment Research Council (NE/D011108/1). Constructive comments from three anonymous referees strengthened the manuscript.

REFERENCES

Andrews, D. G., and M. E. McIntyre, 1976: Planetary waves in horizontal and vertical shear: The generalized Eliassen-Palm relation and the mean zonal acceleration. *J. Atmos. Sci.,* **33,** 2031–2048.

——, J. R. Holton, and C. B. Leovy, 1987: *Middle Atmosphere Dynamics*. International Geophysical Series, Vol. 40, Academic Press, 489 pp.

Boyer, T. P., C. Stephens, J. I. Antonov, M. E. Conkright, R. A. Locarnini, T. D. O'Brien, and H. E. Garcia, 2002: *Salinity*. Vol. 2, *World Ocean Atlas 2001,* NOAA Atlas NESDIS 50, 165 pp.

Cerovecki, I., and J. Marshall, 2008: Eddy modulation of air–sea interaction and convection. *J. Phys. Oceanogr.,* **38,** 65–83.

da Silva, A. M., C. C. Young, and S. Levitus, 1995a: *Anomalies of Heat and Momentum Fluxes*. Vol. 3, *Atlas of Surface Marine Data 1994,* NOAA Atlas NESDIS 8, 413 pp.

——, ——, and ——, 1995b: *Anomalies of Fresh Water Fluxes*. Vol. 4, *Atlas of Surface Marine Data 1994,* NOAA Atlas NESDIS 9, 308 pp.

Fox-Kemper, B., and R. Ferrari, 2008: Parameterization of mixed layer eddies. Part II: Prognosis and impact. *J. Phys. Oceanogr.,* **38,** 1166–1179.

——, ——, and R. Hallberg, 2008: Parameterization of mixed layer eddies. Part I: Theory and diagnosis. *J. Phys. Oceanogr.,* **38,** 1145–1165.

Gill, A. E., 1982: *Atmosphere–Ocean Dynamics*. Academic Press, 662 pp.

Grist, J. P., and S. A. Josey, 2003: Inverse analysis adjustment of the SOC air–sea flux climatology using ocean heat transport constraints. *J. Climate,* **16,** 3274–3295.

Ito, T., J. Marshall, and M. Follows, 2004: What controls the uptake of transient tracers in the Southern Ocean? *Global Biogeochem. Cycles,* **18,** GB2021, doi:10.1029/2003GB002103.

Josey, S. A., E. C. Kent, and P. K. Taylor, 1998: The Southampton Oceanography Centre (SOC) ocean–atmosphere heat, momentum and freshwater flux atlas. Southampton Oceanography Centre Rep. 6, 30 pp.

Kalnay, E., and Coauthors, 1998: The NCEP/NCAR 40-Year Reanalysis Project. *Bull. Amer. Meteor. Soc.,* **77,** 437–471.

Karsten, R., and J. Marshall, 2002: Constructing the residual circulation of the ACC from observations. *J. Phys. Oceanogr.,* **32,** 3315–3327.

Lee, M.-M., D. P. Marshall, and R. G. Williams, 1997: On the eddy transfer of tracers: Advective or diffusive? *J. Mar. Res.,* **55,** 483–505.

LeQuere, C., and Coauthors, 2007: Saturation of the Southern Ocean CO_2 sink due to recent climate change. *Science,* **316,** 1735–1738.

Marshall, D. P., 1997: Subduction of water masses in an eddying ocean. *J. Mar. Res.,* **55,** 201–222.

Marshall, J., and T. Radko, 2003: Residual-mean solutions for the Antarctic Cirumpolar Current and its associated overturning circulation. *J. Phys. Oceanogr.,* **33,** 2341–2354.

——, and ——, 2006: A model of the upper branch of the meridional overturning of the Southern Ocean. *Prog. Oceanogr.,* **70,** 331–345.

Nurser, A. J. G., R. Marsh, and R. G. Williams, 1999: Diagnosing water mass formation from air–sea fluxes and surface mixing. *J. Phys. Oceanogr.,* **29,** 1468–1487.

Olbers, D., and M. Visbeck, 2005: A model of the zonally averaged stratification and overturning in the Southern Ocean. *J. Phys. Oceanogr.,* **35,** 1190–1205.

Simpson, J. H., and J. R. Hunter, 1974: Fronts in the Irish Sea. *Nature,* **250,** 404–406.

Sloyan, B. M., and S. R. Rintoul, 2001: Circulation, renewal, and modification of Antarctic Mode and Intermediate Water. *J. Phys. Oceanogr.,* **31,** 1005–1030.

Smith, S. D., 1988: Coefficients for sea surface wind stress, heat flux, and wind profiles as a function of wind speed and temperature. *J. Geophys. Res.,* **93,** 15 467–15 472.

Speer, K., and E. Tziperman, 1992: Rates of water mass formation in the North Atlantic Ocean. *J. Phys. Oceanogr.,* **22,** 93–104.

——, S. R. Rintoul, and B. Sloyan, 2000: The diabatic Deacon cell. *J. Phys. Oceanogr.,* **30,** 3212–3222.

Stephens, C., J. I. Antonov, T. P. Boyer, M. E. Conkright, R. A. Locarnini, T. D. O'Brien, and H. E. Garcia, 2002: *Temperature*. Vol. 1, *World Ocean Atlas 2001,* NOAA Atlas NESDIS 49, 167 pp.

Thompson, D. W. J., and S. Solomon, 2002: Interpretation of recent Southern Hemisphere climate change. *Science,* **296,** 895–899.

Toole, J. M., 1981: Sea ice, winter convection, and the temperature minimum layer in the Southern Ocean. *J. Geophys. Res.,* **86,** 8037–8047.

Visbeck, M., J. Marshall, T. Haine, and M. Spall, 1997: Specification of eddy transfer coefficients in coarse-resolution ocean circulation models. *J. Phys. Oceanogr.,* **27,** 381–402.

Walin, G., 1982: On the relation between sea surface heat flow and thermal circulation in the ocean. *Tellus,* **34,** 187–195.

Williams, R. G., 1988: Modification of ocean eddies by air–sea interactions. *J. Geophys. Res.,* **93,** 15 523–15 533.